Supporting Information

Layer-by-Layer Fabrication of 3D Hydrogel Structures Using Open Microfluidics

Ulri N. Lee*[,a], John H. Day*[,a], Amanda J. Haack*[,a,b], Ross C. Bretherton[c], Wenbo Lu[a], Cole A. DeForest[§c,d,e,f] Ashleigh B. Theberge[§,a,g], and Erwin Berthier[§,a]

*These authors contributed equally to this work
[a] University of Washington, Department of Chemistry, Seattle, WA
[b] University of Washington School of Medicine, Medical Scientist Training Program, Seattle, WA
[c] University of Washington, Department of Bioengineering, Seattle, WA
[d] University of Washington, Department of Chemical Engineering, Seattle, WA
[e] University of Washington, Institute of Stem Cell & Regenerative Medicine, Seattle, WA
[f] University of Washington, Molecular Engineering & Sciences Institute, Seattle, WA
[g] University of Washington School of Medicine, Department of Urology, Seattle, WA
[§] Email address for correspondence: Erwin Berthier, erwin.berthier@gmail.com; Ashleigh B. Theberge, abt1@uw.edu; Cole A. DeForest, ProfCole@uw.edu

Supporting Information Contents

Extended Materials and Methods

Derivation for SCF condition in rail-based microchannels

In the case where a channel is comprised of multiple surfaces with different materials and unique contact angles, the condition for advancement of a fluid in the channel is given by a condition on the Cassie Angle, θ^*(1a), referred to as the Generalized Cassie law (1b), where f_i is the fraction of the channel's cross-sectional perimeter composed of a material i, and θ_i is the contact angle of material i.

$$\cos(\theta^*) = \sum_i f_i \cos(\theta_i) \quad \text{(Eq. 1a)}$$

$$\cos(\theta^*) > 0 \quad \text{(Eq. 1b)}$$

Given the cross-sectional geometry of a rail-based channel and the convention that the contact angle of fluid on air is $90°$, Eq. 1 can be rewritten as:

(Eq. 2)

Where w_1 is the width of the channel ceiling, w_2 is the width of the channel floor, and h is the distance between the channel ceiling and the floor. Assuming that $w_1 = w_2$, Eq. 2 reduces down to:

$$\frac{h}{w_1} < \frac{\cos(\theta_1) + \cos(\theta_2)}{2} \quad \text{(Eq. 3)}$$

where h is the height of the patterned layer (defined by the distance between the patterning area of the patterning device and the underlying substrate), θ_1 is the contact angle of the patterning device, and θ_2 is the contact angle of the underlying substrate.

Design of hollow double helix

The helix consists of a total of 30 layers of agarose (including the base layer), which were all patterned via SCF and rail-based technology. Each layer looks like a button with two holes, that is rotated about the center for each subsequent layer. Figure S3A illustrates a top-down schematic for the helix design. The length, d, is the diameter of the holes, which is 3 mm for all layers on both sides. r is the distance from the center of the design to the center of the holes on both sides, and for all layers is 2.5 mm. The angle of rotation about the center of the design is denoted by ϕ, and the maximum overhang length is denoted by s. For the first two layers, the angle of rotation, ϕ, is 5° with a designed overhang, s, of 240 μm to establish the overhang. After the overhang was established, the remaining layers were rotated 10° for a total designed maximum overhang of 479 μm. A new device was used for each layer with an alignment marker for consistency in the degree of rotation. The helix was designed to include a curvature that outlined the two holes which allowed for SCF to continue to the edge of the desired overhang. These values can be found in Table S1.

Imaging of hollow double helix

A Nikon DSLR camera was used to take images of the double helix. The helices were removed from the well plate with a spatula and placed on a standard No. 1.5, 25 mm square coverslip (Fisherbrand). A 1 mL syringe with a 18 gauge needle with 18 gauge PTFE tubing attached to reach the bottom of the helices was used to load the helices with dye. A syringe with a 25 gauge needle was used to remove any air

pockets that formed from filling the hollow tubes with dye. During loading, the tubing damaged the walls of the agarose and these irregularities filled with dye (Figure 4C, right). Yellow and blue India ink dye (Dr. Ph. Martin's Bombay India Ink) was used to fill the helix (Figure 4C, right), and dextran with fluorescein 70,000 MW in DI water at 10 mg/mL (Invitrogen) was used to fill a separate helix in Figure 2C. To take the photo in Figure 2C, the fluorescent dye was excited using a 365 nm lamp (Spectroline). Helix images were processed using Adobe Photoshop CC 2018 using a uniform brightness/contrasts adjustment.

Imaging and design of overhanging cross sections

The cross-sectional images shown in Figure 4A were designed such that the overhang and curvature of each layer corresponded to the maximum overhang in the first seven layers of the helix. The curvature information can be found in Table S1 where the first seven layers correspond to the overhang cross section device, as well as the first seven layers of the helix. To image the cross section, a smooth edge was cut using a coverslip (Fisherbrand) and the overhang was transferred to another coverslip for imaging with a DSA25E goniometer (Kruss). The images in Figure 4A are separately constructed agarose structures, cut and imaged at different stages.

Design of curvature for overhanging features

In order to achieve spontaneous capillary flow for all layers of the seven layered overhanging structure (Figure 4A) and the hollow double helix structure (Figure 4C, Figure 2C), the geometry of curvature was adjusted for each layer. If each layer had the same curvature, then the maximum distance (air gap) between the two layers would become great enough that spontaneous capillary flow is inhibited. This concept is illustrated in Figure S3C, as denoted by the red arrow. However, by applying a calculation to change the curvature dimensions of the current layer based upon the dimensions of the previous layer, the distance between layers can be minimized allowing for SCF, illustrated by the reduction of the double-headed red arrow length (Figure S3C). Note that the overhang dimensions for the seven layered overhanging structure in Figure 4A are the same as the dimensions for the first seven layers of the helix. The calculation was made as follows: for the first overhanging layer, layer 2, the radius of curvature is set to 1 mm. Every subsequent layer's radius of curvature is increased by 0.5 mm, i.e., layer 3 is 1.5 mm, layer 4 is 2 mm, etc. Take any layer, n where $n > 1$, and the radius of curvature, r_n is then given by Eq. 4.

$$r_n = 0.5n \qquad \text{(Eq. 4)}$$

Layer 1 has no radius of curvature, as it is not an overhanging layer. The curvature of layer n was designed such that the curvature began at half the distance of the x-component of the previous layer, x_{n-1}, which is illustrated in the diagram below.

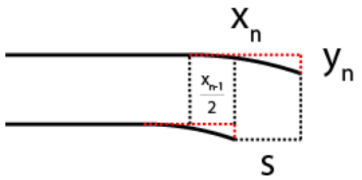

Note that s is the designed maximum overhang, which for the helix design is also denoted by s in Figure S3A. The s component of the curvature for layer n, x_n, is then given by taking one half of the x-component of the previous layer, and adding this to the maximum overhang, s, described in Eq. 5.

$$x_n = \frac{x_{n-1}}{2} + s \quad \text{(Eq. 5)}$$

Note that the maximum overhang, s is set by the angle of rotation for the helix (ϕ in Figure S10A). Using the calculated x-component and the radius of curvature for layer n, the y-component of the curvature can then be derived. The schematic below shows the geometrical schematic to calculate these layers.

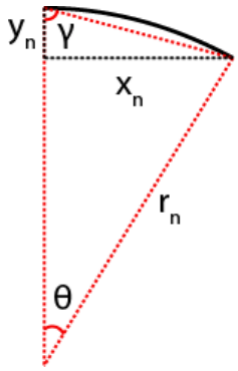

To calculate the angle, θ, which represents the arc angle of the circle that encompasses the curvature, the geometric relation of the radius of curvature, r_n, to the x-component of the curvature was used, and described in Eq. 6 where θ is in degrees.

$$\theta = \arcsin\left(\frac{x_n}{r_n}\right) \quad \text{(Eq. 6)}$$

Using this angle and the fact that the red dotted triangle is an isosceles triangle, the value of angle γ could be calculated using Eq. 7, where γ and θ are in degrees.

$$\gamma = \frac{180 - \theta}{2} \quad \text{(Eq. 7)}$$

Then, the value of y_n can be calculated using Eq. 8.

$$y_n = \frac{x_n}{\tan(\gamma)} \quad \text{(Eq. 8)}$$

These calculations were applied to all layers to derive the values in Table S1. Note that the first overhanging layer, layer 2, was set such that the curvature began at the edge of layer 1.

Enzymatically degradable hydrogels synthetic information

Chemical reagents were obtained from either Sigma-Aldrich or Fisher Scientific unless otherwise noted. Amino acids for peptide synthesis were purchased from ChemPep and associated coupling reagents from Chem-Impex.

Peptides were synthesized using standard Fmoc Solid Phase Peptide Synthesis (SPPS) on a microwave-assisted Liberty1 automated peptide synthesizer. Fmoc groups were deprotected in 20% piperidine (v/v) in N,N dimethylformamide (DMF) with 0.1 M 1-hydroxybenzotriazole (HOBt) at 90°C for 90 seconds. Fmoc-protected amino acids (1 mmol; 4x) were coupled in a solution of 1-[Bis(dimethylamino)methylene]-1H-1,2,3-triazolo[4,5-b]pyridinium 3-oxide hexafluorophosphate (HATU; 1 mmol; 4x) and diisopropylethylamine (DIEA; 2 mmol; 8x) in a mixture of 20% N-methyl-2-pyrrolidone (NMP) in DMF at 75°C for 5 minutes.

Semi-preparative scale reversed-phase high-pressure liquid chromatography (RP-HPLC) was conducted on a Dionex Ultimate 3000 with 220 nm and 280 nm detection wavelengths, through a Thermo 5 μm Sychronis silica 250x21.2 mm C18 column. Pure fractions were lyophilized using a LABCONCO FreeZone 2.5 plus freeze-dryer equipped with a LABCONCO rotary vane 117 vacuum pump. Matrix-assisted laser desorption/ionization time of flight (MALDI-TOF) mass spectrometry was performed on samples suspended in a matrix of α-cyano-4- hydroxycinnamic acid:2,5-dihydroxy benzoic acid (2:1) using a Bruker AutoFlex II mass spectrometer in reflectron positive mode with detector range set to 600-3000 Da.

Four-arm poly(ethylene glycol) (MW = 20,000 Da) end-functionalized with bicyclononyne (PEG-tetraBCN) and N_3-GRGDS-NH_2 peptide were synthesized as previously described [1,2].

Recombinant Expression and Purification of SrtA(5M)

pET30b-5M SrtA was a gift from Hidde Ploegh (Addgene plasmid # 51140 ; http://n2t.net/addgene:51140 ; RRID:Addgene_51140). Chemically competent BL21 *E. coli* cells were transformed with the pET30b-5M SrtA plasmid, expanded in 1 L of Luria broth at 37°C under agitation at 200 RPM, and induced using 0.5 mM Isopropyl-beta-D-thiogalactoside when OD600 of the bacterial culture reached 0.6, measured on a Thermo Fisher Nanodrop 2000 spectrophotometer. After overnight culture at 17°C and 200 RPM agitation, cells were pelleted, resuspended in lysis buffer (20 mM Tris; 50 mM NaCl; 10 mM imidazole; 40 mL) on ice, and lysed by sonication (6 x 3 min cycles; 30% amplitude, 33% duty cycle and 3 min resting). The soluble lysate fraction was incubated with 3 mL Ni-NTA Agarose Beads (GoldBio) for 1hr at 4°C in a gravity column. The resin and bound His-tagged protein were washed in wash buffer (20 mM Tris; 50 mM NaCl; 20 mM imidazole; 5 x 20 mL), then purified SrtA was eluted in elution buffer (20 mM Tris; 50 mM NaCl; 20 mM imidazole; 20 x 1 mL). Protein was then dialyzed against PBS with Thermo Fisher SnakeSkin Dialysis Tubing (MWCO ~10 kDa) to remove Tris and imidazole. Protein was then spin concentrated in an Amicon centrifugal column (MWCO ~10 kDa), glycerol was added to 20% wt/vol, and aliquots were stored at -80°C prior to use. Protein identity and purity were confirmed using SDS-PAGE and whole protein ESI-MS (Expected 17.8 kDa, Observed 17.8 kDa).

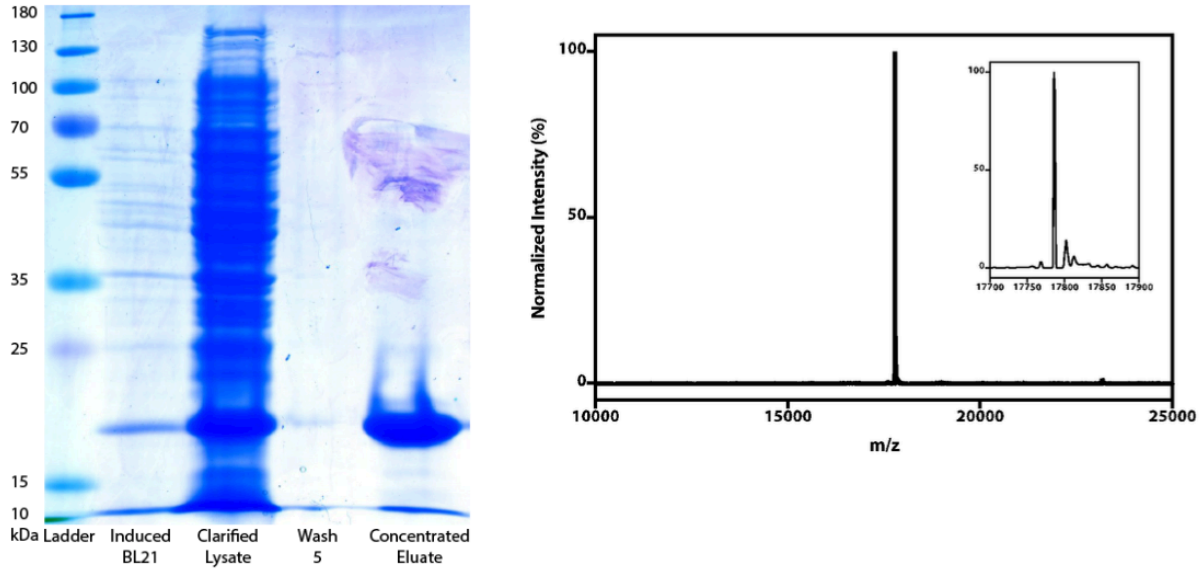

SrtA(5M) protein purification was evaluated by SDS-PAGE, revealing a strong 18 kDa band corresponding to the protein (left). Protein Identity was verified by mass spectrometry (right).

Synthesis of N_3-RGPQGIWGQGRK(N_3)-NH_2 and N_3-RGPQGIWGQLPETGGRK(N_3)-NH_2

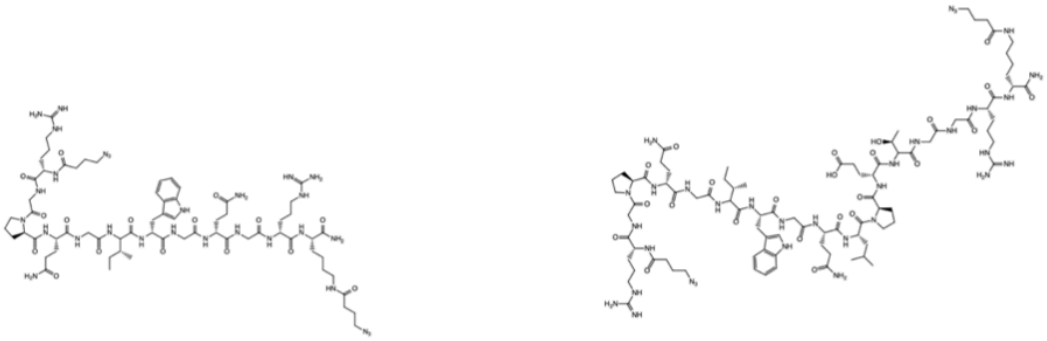

Chemical structures of the MMP-degradable peptide N_3-RGPQGIWGQGRK(N_3)-NH_2 (left) and the MMP OR SrtA degradable peptide N_3-RGPQGIWGQLPETGGRK(N_3)-NH_2 (right)

The peptides H-RGPQGIWGQGRK(Dde)-NH_2 and H-RGPQGIWGQLPETGGRK(Dde)-NH_2 were synthesized by Fmoc SPPS at 0.25 mmol scale on rink amide resin. The Dde protecting group was cleaved from resin-bound peptide using 2% hydrazine (3 x 10 min). 4-azidobutanoic acid (4x; 259 mg; 2 mmol) was conjugated to the free amines on the N-terminus and deprotected Lysine though *in situ* ester activation using a solution of HATU (3.95X; 750 mg; 1.97 mmol) and diisopropylethylamine (DIEA; 8X; 1.38 mL; 4 mmol) for 90 minutes [1]. Resin was then thrice washed with DMF and thrice with dichloromethane (DCM) prior to peptide cleavage from resin [95%/2.5%/2.5% Trifluoracetic Acid (TFA)/ Triisopropylsilane (TIS)/ H_2O]. Crude peptide product was precipitated in ice-cold diethyl ether and dried under N_2 prior to purification by RP-HPLC (55-minute gradient of 5-100% acetonitrile in water). Lyophilization yielded the pure final

products (N_3-RGPQGIWGQGRK(N_3)-NH_2 and N_3-RGPQGIWGQLPETGGRK(N_3)-NH_2), each as a light-yellow solid. Peptide identity was confirmed using MALDI-TOF.

Peptide Sequence	Expected Mass (Da)	Observed Mass (Da)	Yield (mg)	Yield (mmol)	Yield (%)
N_3-RGPQGIWGQGRK(N_3)-NH_2	1559.83	1560.36	52.5	0.033	13.2
N_3-RGPQGIWGQLPETGGRK(N_3)-NH_2	2056.08	2058.47	51.2	0.025	9.9

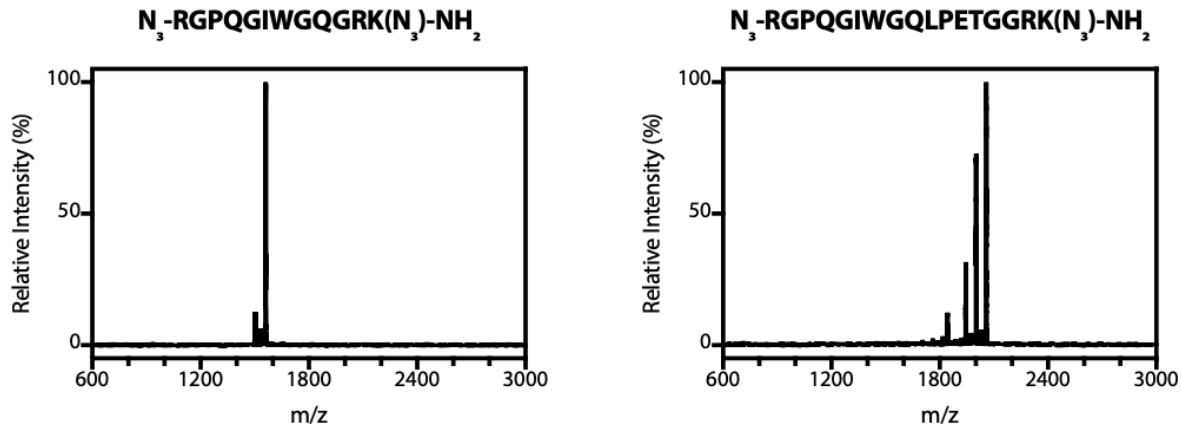

MALDI mass spectra for the synthesized and HPLC purified peptides.

Preparation of Patterning Rails for cell-encapsulated PEG hydrogel patterning.
Rails were printed with a Form 2 3D printer. Devices were sterilized under UV light for 1 hour. To prevent hydrogel or cell adhesion, the devices were incubated in 1% Bovine Serum Albumin (BSA) for 1-2 hours, and allowed to fully air dry prior to use.

References

1. DeForest, C.A.; Tirrell, D.A. A photoreversible protein-patterning approach for guiding stem cell fate in three-dimensional gels. *Nat. Mater.* **2015**, *14*, 523–531.
2. Arakawa, C.K.; Badeau, B.A.; Zheng, Y.; DeForest, C.A. Multicellular Vascularized Engineered Tissues through User-Programmable Biomaterial Photodegradation. *Adv. Mater.* **2017**, *29*, 1703156.
3. Bellis, S.L. Advantages of RGD peptides for directing cell association with biomaterials. *Biomaterials* **2011**, *32*, 4205–4210.

Supplementary Figures

Note: Supplementary Figures S1-4 are demonstrations of the resolution in agarose structures achievable with the Form 2 3D printer that we used to fabricate the rail structures and is not inherent to the 3D patterning method presented in this paper.

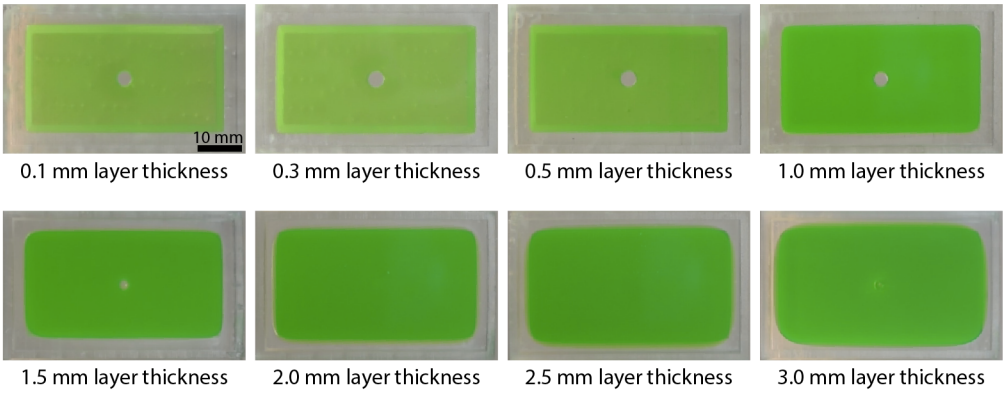

Figure S1. Effects of increasing layer thickness on capillary pinning at corners. At layer thickness 0.1, 0.3, and 0.5 mm the agarose fully fills to the corner of the patterning device. At 1.0 mm and above, agarose is unable to pin at the corners of the patterning device. Images are taken from the underside of single layers of patterned agarose. Images are representative of n=3.

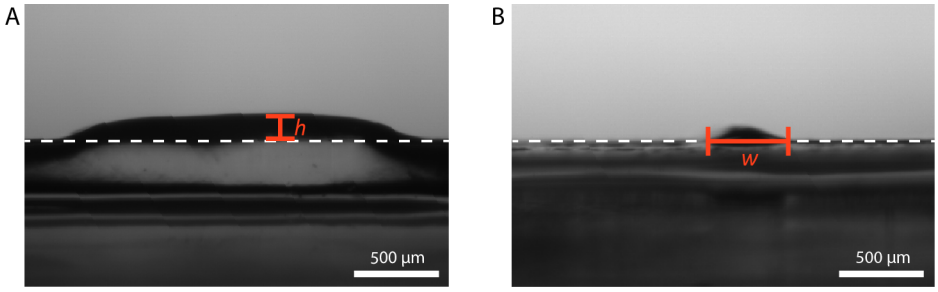

Figure S2. Cross-sectional images of minimum height and width of a layer. (A) Minimum layer height, *h*, was meausred from the baseline (dotted line) to the highest point on the gel layer. The average minimum height was 140 ± 19 µm. (B) Minimum feature width, *w*, was measured at the base of the top layer. The average minimum width was 660 ± 210 µm. At larger widths there was better control over deviations in the width (1292 ± 46 µm). All data are reported as mean ± SD for n=3.

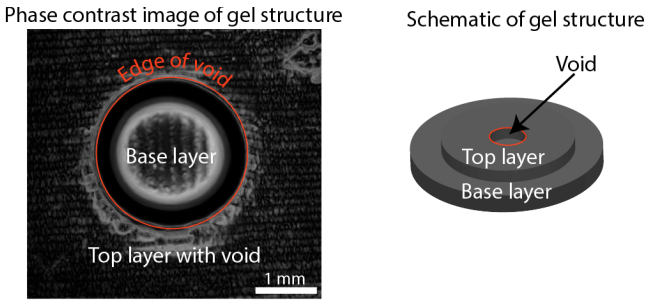

Figure S3. Minimum diameter of void. Red indicates the circle used to measure the diameter of the void. Minimum diameter of void is 1256 ± 18 µm. Data are reported as mean ± SD for n=3. Phase contrast images were taken with a Zeiss Primovert inverted microscope with a MU1403B camera (AmScope).

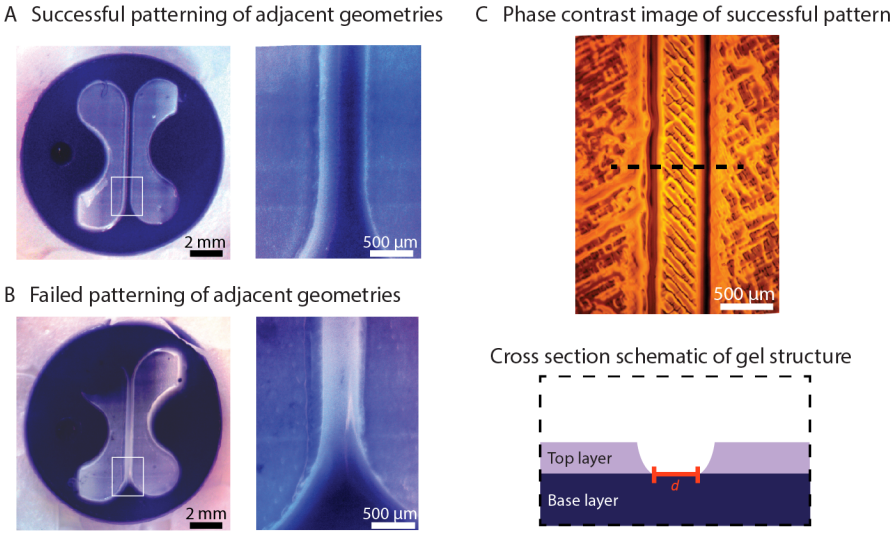

Figure S4. Minimum spacing between two independently patterned geometries (white) over a base layer of gel (purple) is 270 ± 49 µm. (A) Successful patterning of adjacent geometries. (B) Failed patterning of adjacent geometries. (C) Representative image of phase contrast image of agarose structure. Dotted line indicates cross section of the gel in schematic where *d* indates the area of measurement on the gel. Phase contrast images were taken with a Zeiss Primovert inverted microscope with a MU1403B camera (AmScope). All data are reported as mean ± SD for n=3.

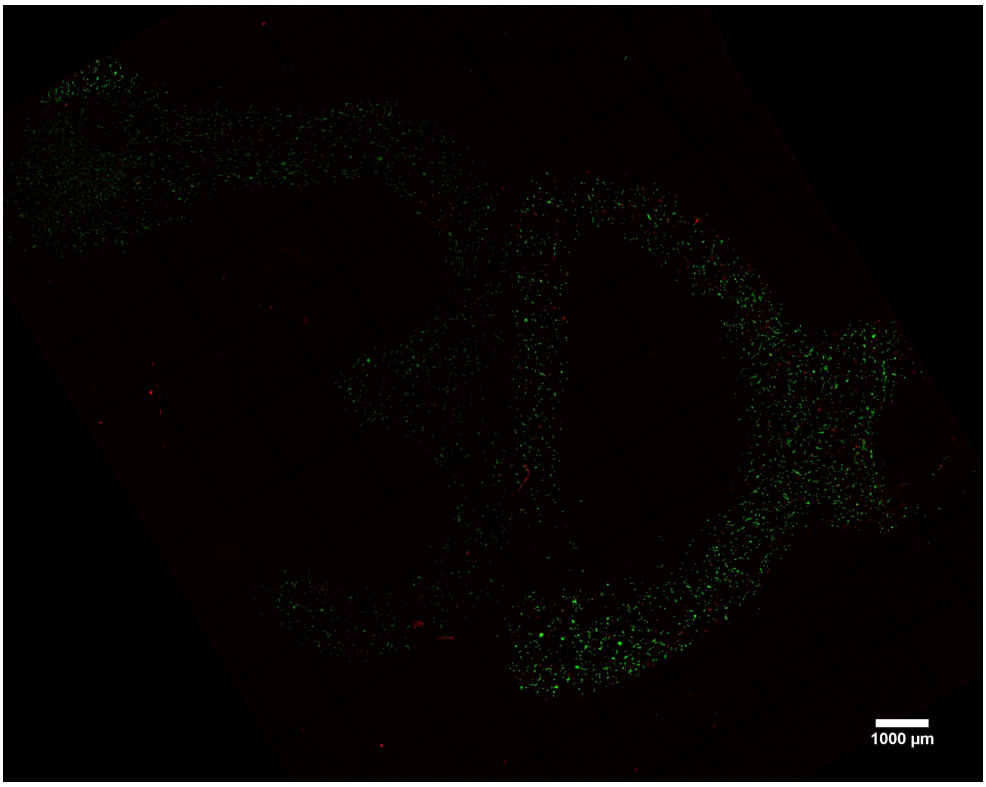

Figure S5. Confocal images showing live/dead staining of human fetal lung fibroblast cells in 3D collagen structure from Figure 6. Image comprises 130 fields of view (which each contain 27 Z-stacked images) stitched together. Green is Calcein AM, which stains the cytoplasm of live cells, and red is ethidium homodimer, which stains the nuclei of dead cells. Viability (87% over all, 93% and 86% in the '3' and D' patterns, respectively) was quantified in FIJI image processing software (using a minimum cell area of 25 px^2 for the live and dead stains and a minimum circularity of 0.25 for the dead stain).

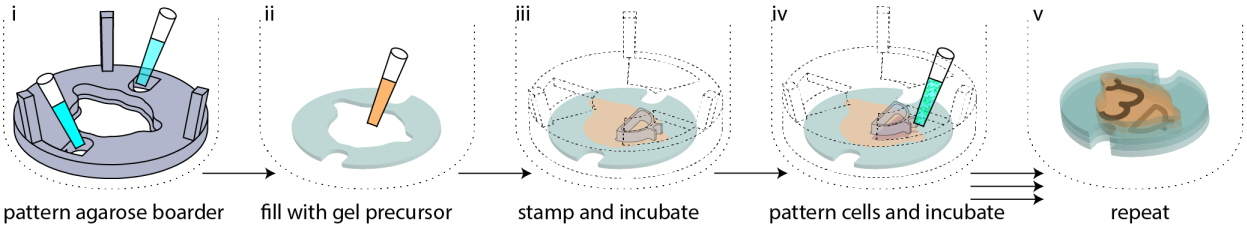

Figure S6. Schematic workflow of agarose and collagen patterning process used to make the cell-laden collagen structure structure in Figure 6. (i) A 200 μm tall agarose border is patterned in a 6-well plate. (ii) The agarose border is then filled with collagen gel precursor. (iii) A 200 μm tall 'D' patterning device is then placed in the well, which precisely sets the height of the collagen fill to 200 μm (the patterning device is shown as two parts for visualization purposes, where the main device component is shown in dotted lines and the 'D' patterning component is shown in transparent grey). The well plate is then incubated with the device in place for 10 minutes to polymerize the collagen. (iv) The previous patterning device is then removed, and an identical, 300 μm tall patterning device is placed in the same position. 8 μL of cell-laden collagen gel precursor solution is then pipetted into the loading region of the patterning device, at which point the gel precursor solution flows through the 'D' pattern. These 4 steps are repeated once more with a '3' pattern, and then again with no pattern to yield (v) the final structure. As described in the manuscript, the final structure consists of a first cell-free layer that is 200 μm tall, then a cell-laden collagen layer containing the 'D' pattern that is 100 μm tall, then a cell-free layer that is 200 μm tall, then a finally cell-laden collagen '3' pattern that is 100 μm tall, then a cell-free layer.

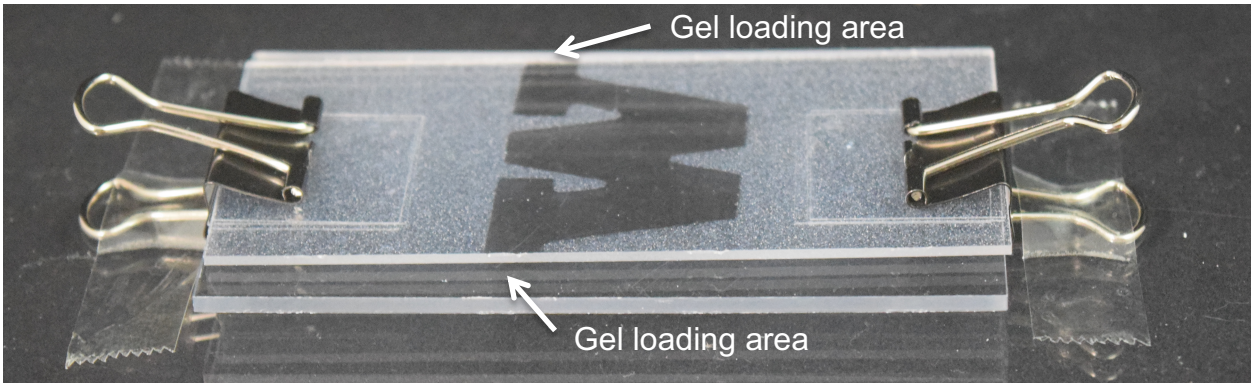

Figure S7. Set up of Figure 8Aii before pre-gel solution is pipetted into gel loading areas.

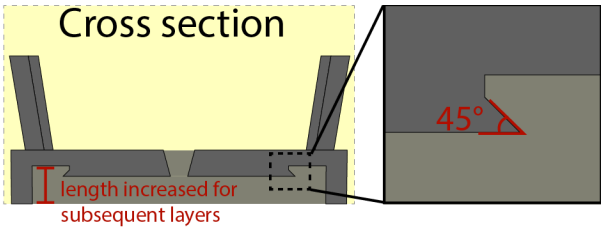

Figure S8. Cross section of patterning device with inset of 45° angled edge to prevent capillary rise. If the patterning device contained a simple 90° angled edge rather than the 45° angled edge shown here, the pre-gel solution would wet the vertical edge of the patterning device due to capillary rise. The diagram also shows the portion of patterning device that is adjusted to increase the height of the patterning area for subsequent layers of hydrogel.

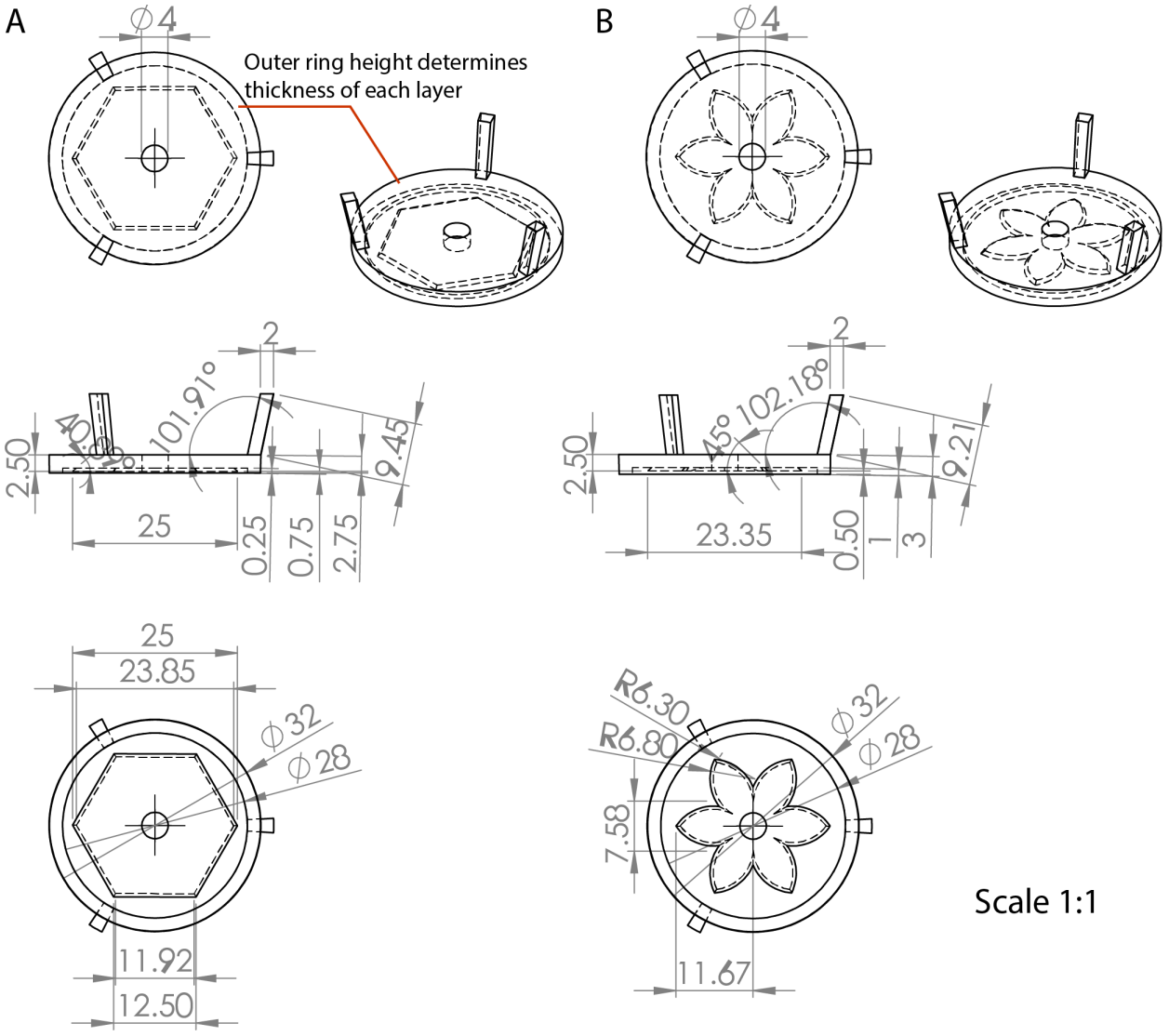

Figure S9. Schematic diagrams illustrating the dimensions of the patterning devices in Figure 2B. All dimensions are in mm. CAD files are also included. (A) First layer hexagon pattern. Red lines indicate the ring ('foot' of the device) that sits flush to the well plate floor which is adjusted for each patterning device to determine layer thickness. (B) Second layer flower pattern.

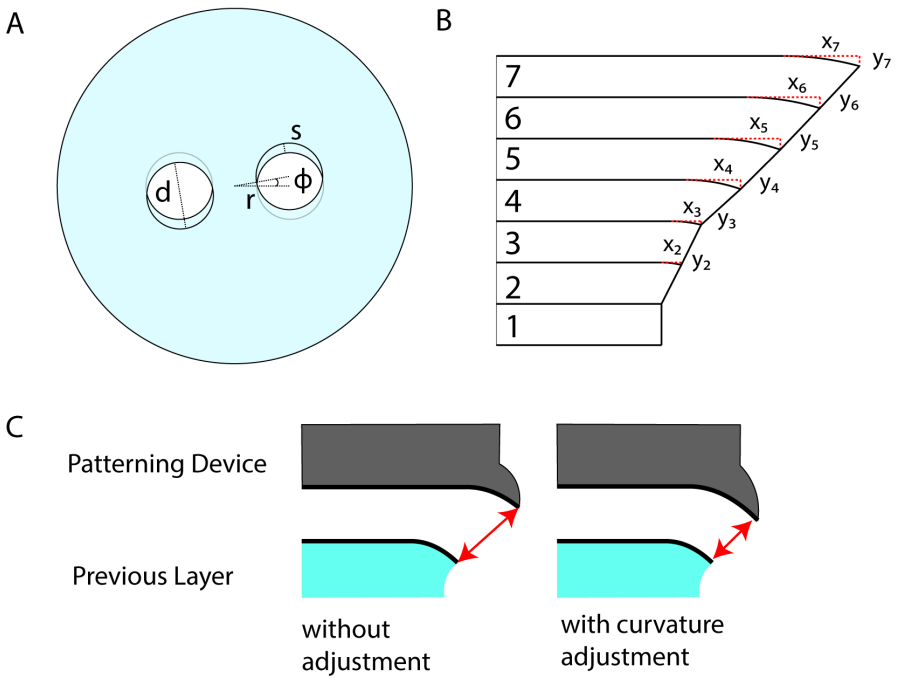

Figure S10. Schematic of helix and overhang design used to make the structures shown in Figure 4 of the manuscript. (A) Dimensions of each design parameter where d is diameter of hole, r is distance from center of the design to the center of the hole, ϕ is the angle of rotation from layer to layer, and s is the maximum overhang length. (B) Schematic of the overhang design for 7 layers, showing the curvatures for each layer. Note: there is no curvature for the first layer. (C) The effect of adjusting the curvature based on the previous curvature on the distance between the two layers, as denoted by the red arrows, which limits the surface capillary flow to the edge of the overhang. The left diagram shows the same curvature for both layers and the right diagram shows curvature adjustment on the patterning device based on the previous layer,

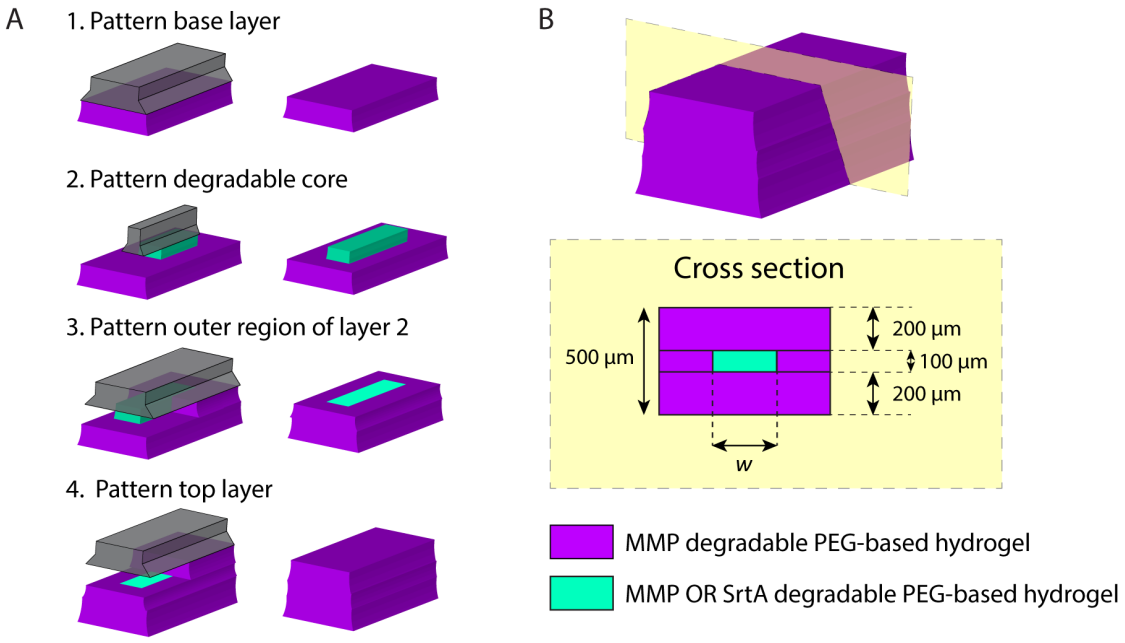

Figure S11. 3D open microfluidic fabrication of PEG-based structure with a enzymatically degradable core. (A) Workflow of fabrication. The gel structure was fabricated in four steps to create a three layered structure consisting of a matrix metalloproteinase (MMP) OR sortase (SrtA) degradable core (teal gel) surrounded entirely by a MMP only degradable gel (purple gel). The middle layer consisting of the core was patterned in two steps, with the SrtA OR MMP degradable core patterned first. (B) Cross section showing dimensions of gel. The total height was designed as 500 μm with the middle layer designed as 100 μm. The width of the core, *w*, was either 1.0 mm or 0.5 mm.

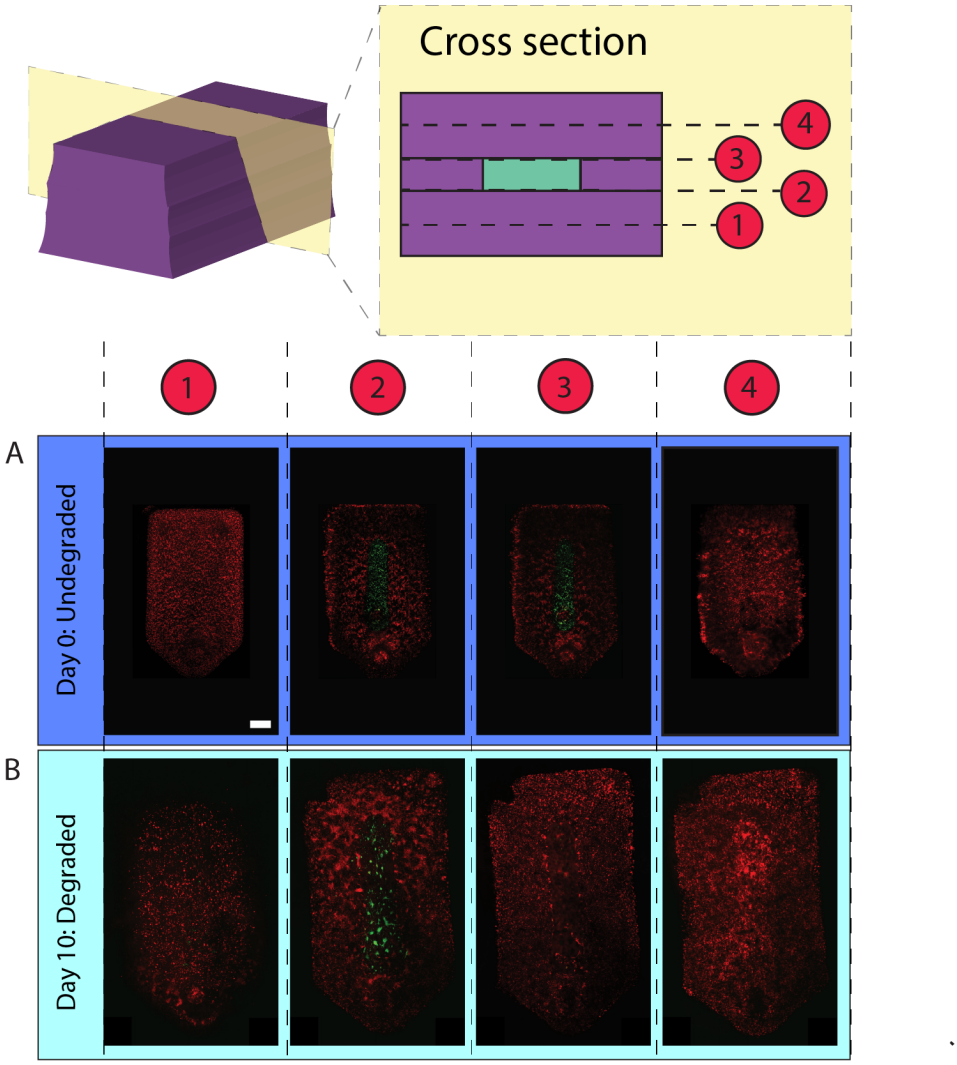

Figure S12. Confocal slices of multiple top-down views of the structure shown in Figure 7. Slice 1-4 is denoted on the cross section schematic with dotted lines. (A) Slices taken from gel just after encapsulation and patterning with no SrtA degradation. (B) Slices taken from gel on day 10 of culture, after SrtA degradation on day 5. eGFP expressing cells are not found in at the top of the middle layer (cross section 3), as the cells have settled to the bottom of the cavity. Scale bar is 1 mm.

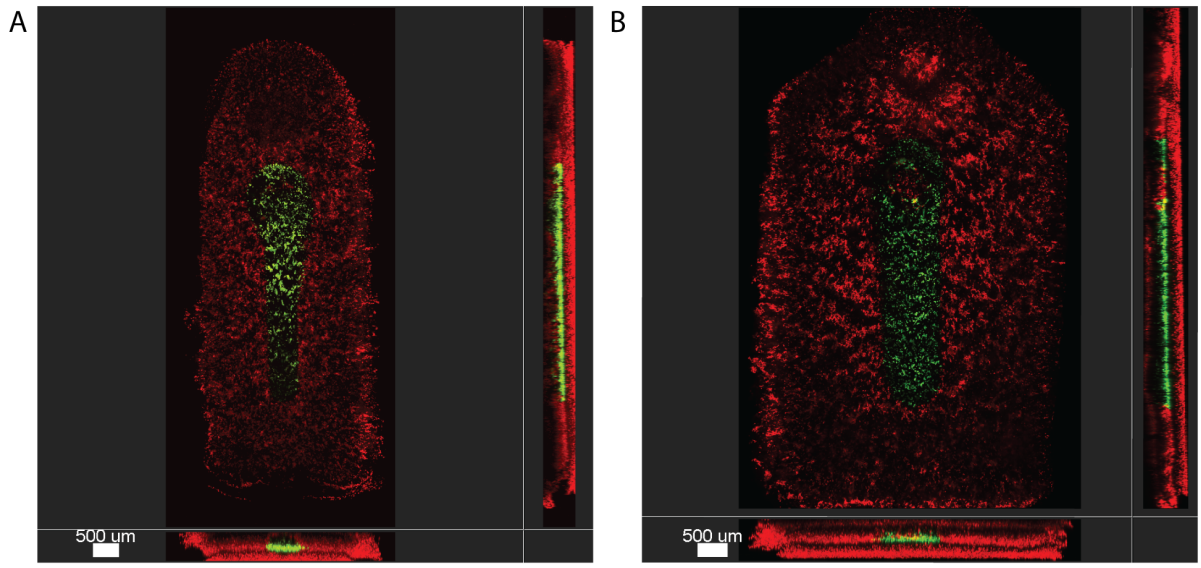

Figure S13. Confocal images of different degradable core geometries. (A) Degradable core width designed with a width of 0.5 mm, and the outside structure was designed with a width of 2.5 mm (B) Degradable core width designed with a width of 1.0 mm with an outside structure designed with a width of 4.5 mm. Scale bars apply to all planes of imaging.

Table S1. Calculated designed curvature values for all patterning devices used for double helix structure.*

Layer	Rotation angle, ϕ (degree)**	Maximum overhang*** (μm)	Radius of curvature (mm)	Horizontal length of curvature, x (μm)	Vertical length of curvature, y (μm)
1	0	0	0	0	0
2	5	239.9	1.0	239.9	29.2
3	5	239.9	1.5	359.9	43.8
4	10	479.4	2.0	659.3	111.8
5	10	479.4	2.5	809.1	134.5
6	10	479.4	3.0	884.0	133.2
7	10	479.4	3.5	921.4	123.5
8	10	479.4	4.0	940.1	112.0
9	10	479.4	4.5	949.5	101.3
10	10	479.4	5.0	954.2	91.9
11	10	479.4	5.5	956.5	83.8
12	10	479.4	6.0	957.7	76.9
13	10	479.4	6.5	958.3	71.0
14	10	479.4	7.0	958.6	65.9
15	10	479.4	7.5	958.7	61.5
16	10	479.4	8.0	958.7	57.7
17	10	479.4	8.5	958.7	54.2
18	10	479.4	9.0	958.7	51.2
19	10	479.4	9.5	958.7	48.5
20	10	479.4	10.0	958.7	46.1
21	10	479.4	10.5	958.7	43.9
22	10	479.4	11.0	958.7	41.9
23	10	479.4	11.5	958.7	40.0
24	10	479.4	12.0	958.7	38.4
25	10	479.4	12.5	958.7	36.8
26	10	479.4	13.0	958.7	35.4
27	10	479.4	13.5	958.7	34.1
28	10	479.4	14.0	958.7	32.9
29	10	479.4	14.5	958.7	31.7

*First seven layers curvature and overhang information also corresponds to the cross section device in Figure 4A.
**Rotation angle represents the rotation change from the previous layer. Values are in degrees.
***Maximum overhang corresponds to s in Figure S10A.